Available online at www.sciencedirect.com

SciVerse ScienceDirect

Procedia Engineering 00 (2015) 000–000

Procedia Engineering

www.elsevier.com/locate/procedia

The 13th Hypervelocity Impact Symposium

# HVI ballistic limit characterization of fused silica thermal panes

J. E. Miller[a,b]*, W. E. Bohl[d], E. L. Christiansen[c], B. A. Davis[b], and K. D. Deighton[d]

[a]*CASSMAR, University of Texas at El Paso, 500 W. University Ave., El Paso, TX 79968*
[b]*Jacobs, NASA Johnson Space Center, 2101 NASA Parkway, Houston, TX 77058*
[c]*NASA Johnson Space Center, 2101 NASA Parkway, Houston, TX 77058*
[d]*Lockheed Martin, 2100 Space Park Drive, Houston, TX 77058*

**Abstract**

Fused silica window systems are used heavily on crewed reentry vehicles, and they are currently being used on the next generation of US crewed spacecraft, Orion. These systems improve crew situational awareness and comfort, as well as, insulating the reentry critical components of a spacecraft against the intense thermal environments of atmospheric reentry. Additionally, these materials are highly exposed to space environment hazards like solid particle impacts. This paper discusses impact studies up to 10 km/s on a fused silica window system proposed for the Orion spacecraft. A ballistic limit equation that describes the threshold of perforation of a fuse silica pane over a broad range of impact velocities, obliquities and projectile materials is discussed here.


*Keywords*: multi-shock shield, catalogued debris, fabric shield

**Nomenclature**

| | |
|---|---|
| $C$ | Sound speed (km/s) |
| $d$ | Diameter (cm) |
| $R$ | Residual thickness (cm) |
| $t$ | Thickness (cm) |
| $u$ | Particle velocity (km/s) |
| *Symbols* | |
| $\theta$ | Angle |
| $\rho$ | Density (g/cm$^3$) |
| *Subscripts* | |
| $c$ | Critical |
| $i$ | Impact |
| $G$ | Glass |

## 1. Introduction

Fused silica window systems are frequently used on crewed reentry vehicles for crew situational awareness and comfort and to insulate against the reentry plasmas generated by atmospheric braking from orbital and exo-orbital velocities. To prevent hot plasma from entering volumes of the spacecraft that contain critical reentry components, it is important that flow paths that allow rapid movement of reentry plasmas are blocked even after exposure to space environment threats like orbital debris and meteoroids [1]. Owing to the brittle nature of fused

* Corresponding author. Tel.: +1-281-244-8093; fax: +1-281-.
*E-mail address:* joshua.e.miller@nasa.gov.

silica windows, large flow paths are possible even with small impacting particles; consequently, there is a need to characterize the limiting performance of fused silica windows.

The Multi-Purpose Crew Vehicle (MPCV), like its predecessors, will also use windows for crew comfort and situational awareness. The MPCV is being designed with a redundant acrylic thermal pane to make the vehicle more survivable to the solid particle environment; however, reliability of the vehicle is being tied to the performance of the fused silica window system. Owing to the presence of the redundant thermal pane of the window system, the MPCV is considered reliable to perform its reentry mission with flight induced damage from the solid particle environment up to perforation of the fused silica pane. To characterize the window system's response a test and analysis effort has been performed by the NASA Johnson Space Center's Hypervelocity Impact Technology Laboratory (HVIT) and Lockheed Martin Space Systems Company (LMSSC), to quantify the damage obtained in fused silica panes from test and analysis for use in system reliability assessments.

In the testing reported here, fused silica material carried over from the orbiter program has been impacted with spherical projectile materials typical of the orbital debris environment and surrogate to the meteoroid environment to determine the depth of penetration. These tests have been performed at NASA Johnson Space Center's remote White Sands Test Facility two-stage gas guns to $\gtrsim 8$ km/s and at University of Dayton Research Institute's three-stage gas gun to $\sim 10$ km/s [2]. Both facilities are capable of precision measurements of pre-test projectiles, impact velocities to ±0.2 km/s and projectile integrity verification prior to impact. The post-test characterizations are performed by HVIT. The testing has also been augmented by simulations performed with Sandia National Laboratories three dimensional hydrodynamics simulation tool CTH version 9.1 performed by the authors. The accumulated test and simulation data have been consolidated into a threshold perforation equation for fused silica glass discussed here.

## 2. Materials & Methods

Thirteen impact tests into the fused silica window systems for the Orion spacecraft, shown in Fig. 1, have been performed to bracket the onset of perforation of fused silica glass. The impact test article consists of an outer ½" (1.27 cm) fused silica pane that is 10" (25.4 cm) in diameter and an inner ⅝" (1.59 cm) acrylic pane that is 9" (22.9 cm) in diameter. The two panes are separated from each other by a gap of ½" (1.27 cm), which is allowed to vent to vacuum. An illustration of this configuration is shown in Fig. 1a. The fused silica pane and the acrylic pane are constrained in an aluminum frame with rubber gaskets (to prevent metal-to-glass contact) as shown in Fig. 1b. There are four layers of ⅛" (0.318 cm) thick rubber gasket between the window an acrylic material to produce the ½" (1.27 cm) standoff.

Impact tests have been performed into the fused silica panes using aluminum, nylon and steel spherical projectiles with impact speeds from 3 to 10 km/s and impact obliquity angles of 0° and 45° as measured between the projectile velocity vector and window system normal. These impacts produce a penetration and spall crater with images and records from the HVIT shot database shown in Fig. 2. With the images, the impact conditions are given for most of the tests and includes the projectile material and size, the impact speed and impact obliquity angle. In addition to the impact characteristics, Fig. 2 shows the residual depth of the pane when no perforation occurs which is defined here as the thickness of the pane less the maximum penetration crater depth (depth of removed material on the impact side of the window) and spall crater depth (depth of removed material on the opposite surface of the window) that have been obtained using a Keyence LK-G152 laser depth finder.

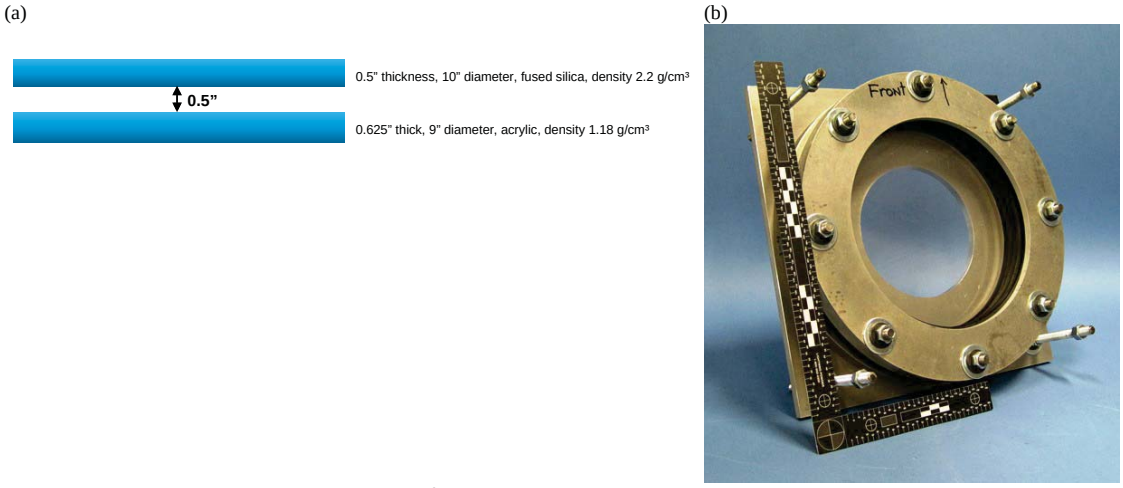


Fig. 1. Window test article assembly (a) ½" configuration diagram (not to scale) and (b) oblique view ½" representative test article.

**HITF14075**
3.18 Nylon mm @ 7.15 km/s & 0°
Residual thickness = 4.7 mm

**HITF14076**
2.80 mm Al2017 @ 3.97 km/s & 0°
Residual thickness = 4.1 mm


**HITF14078**
2.50 mm Al2017 @ 7.04 km/s & 45°
Residual thickness = 0.2 mm

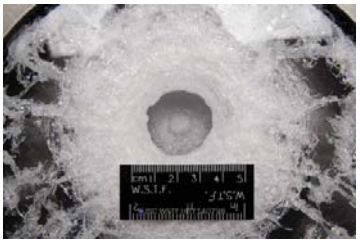

**HITF14079**
3.58 mm Nylon @ 7.16 km/s & 0°
Perforation

**HITF14080**
3.58 mm Nylon @ 7.14 km/s & 45°
Perforation

**HITF14081**
1.40 mm SS440C @ 4.11 km/s & 0°
Residual thickness = 8.4 mm

**HITF14082**
2.50 mm Al2017 @ 7.23 km/s & 0°
Perforation

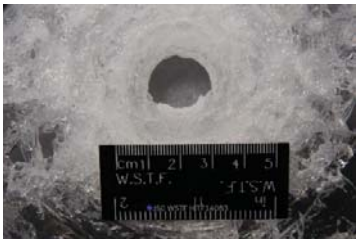

**HITF14083**
2.80 mm Al2017 @ 7.10 km/s & 45°
Perforation


**HITF14084**
2.20 mm Al2017 @ 7.22 km/s & 0°
Residual thickness = 2.7 mm

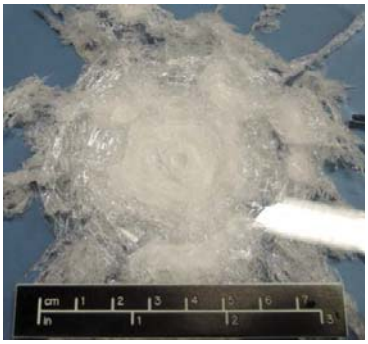

**HITF13243**
2.38 mm Nylon @ 9.23 km/s & 0°
Residual thickness = 5.4 mm

**HITF13244**
1.40 mm Al2017 @ 9.89 km/s & 0°
Residual thickness = 7.7 mm

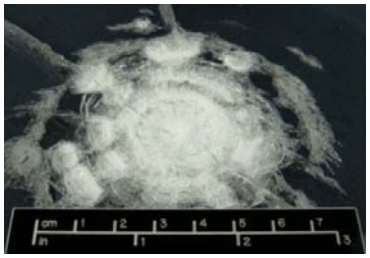

**HITF13245**
1.00 mm SS 440C @ 9.56 km/s & 0°
Residual thickness = 5.3 mm

Fig. 2. Imagery of the window assembly tests with test details of the impactor diameter and impact conditions including the measured residual thickness.

## 3. Theory

Simulations have also been performed using the CTH hydrodynamic simulation tool version 9.1 to expand the obtained dataset. In the simulations, the window configuration of Fig. 1 has been considered for impacts into ½" (1.27 cm) thick fused silica. The simulations used a fixed three dimensional cubic mesh with spatial resolution of 75 μm and infinite boundary conditions. The model extends 3 cm from the impact site in the directions normal to the projectile flight path.

The constitutive models, equation of state (bulk properties) and strength (deviatoric properties), have been developed for the materials in the simulation using CTH data inputs as much as possible. The projectiles that are used in the simulations all used native models from CTH except nylon which does not have native strength and fracture models. The Al2017-T4 projectiles use the aluminum Mie-Gruneissen equation of state referenced to the principal Hugoniot for Al2024-T4. The bulk modulus determined from the zero intercept of the principal Hugoniot is 76.2 GPa, and all other moduli are determined by assuming a homogeneous, isotropic material using the Poisson ratio of 0.33. The strength model is the native CTH Johnson-Cook model for Al2024-T4. The fracture model used is the hydrostatic tensile limit taken to be 427 MPa. The nylon projectiles use the nylon Mie-Gruneissen equation of state for nylon referenced to the principal Hugoniot for nylon to describe the bulk properties. The bulk modulus from the model is 7.5 GPa. The elastic/perfectly-plastic vonMises strength model is used with the yield strength of 25 MPa and a Poisson ratio of 0.4. After yield, the material is assumed to be perfectly plastic until the hydrodynamic tensile limit of 75 MPa is reached where the material is assumed to fail by the insertion of void. The steel projectiles use the Mie-Gruneissen equation of state for alpha phase iron with energy and scaled to 7.65 g/cm$^3$. The modeled bulk modulus is 162 GPa. The moduli are determined from a Poisson ratio of 0.29. The Johnson-Cook model for 1050 steel is used in the analysis with hydrostatic tensile limit of the steel projectile taken as 2.083 GPa.

The fused silica model uses a modified Johnson-Holmquist (JH) ceramic model derived from a float glass model native to CTH. A comparison of the existing float glass model and the as-run fused silica model are given in Table 1 and Table 2 for bulk and deviatoric properties, respectively. As can be seen, only JHRHO (density) and JHSHRM (shear modulus) are different between the two models [3].

Table 1 Comparison of the JH ceramic model for float glass to the fused silica model for bulk properties

| Parameter | Float glass value | Units | Fused silica value | Units |
|---|---|---|---|---|
| **JHK1** | 45.4 | GPa | 45.4 | GPa |
| **JHK2** | -138 | GPa | -138 | GPa |
| **JHK3** | 290 | GPa | 290 | GPa |
| **JHRHO** | 2.53 | g/cm$^3$ | 2.204 | g/cm$^3$ |
| **JHCV** | 974 | J/kg/K | 974 | J/kg/K |
| **JHSHRM** | 30.4 | GPa | 31.4 | GPa |
| **JHHEL** | 5.95 | GPa | 5.95 | GPa |

Table 2 Comparison of the JH ceramic model for float glass to the fused silica model for deviatoric properties

| Parameter | Float glass value | Units | Fused silica value | Units |
|---|---|---|---|---|
| **JHT** | -150 | MPa | -150 | MPa |
| **JHK1** | 45.4 | GPa | 45.4 | GPa |
| **JHBETA** | 1 | | 1 | |
| **JHRHO** | 2.53 | g/cm$^3$ | 2.204 | g/cm$^3$ |
| **JHSHRM** | 30.4 | GPa | 31.4 | GPa |
| **JHA** | 0.93 | | 0.93 | |
| **JHB** | 0.88 | | 0.88 | |
| **JHC** | 0.003 | | 0.003 | |
| **JHD1** | 0.053 | | 0.053 | |
| **JHD2** | 0.85 | | 0.85 | |
| **JHM** | 0.35 | | 0.35 | |
| **JHN** | 0.77 | | 0.77 | |
| **JHSFMAX** | 2.975 | GPa | 2.975 | GPa |
| **POISSON** | 0.25 | | 0.25 | |

Simulations have been performed to compare the output from the simulation model with the observed results as shown in Fig. 3 carried out to 25 μs as determined to be the cessation of crater and spall development using time lapse output of the fused silica pane. In the figure the relevant observed test damage image is repeated from Fig. 2 as a comparison to the final density contour from the simulation. While the test articles have not been sectioned for a direct profile comparison, the measurements of the crater depth and the spall depth can be compared. HITF13243 performed with a 2.38 mm nylon projectile at 9.23 km/s is compared to a nylon simulation with a 2.4 mm projectile at 9.23 km/s in Fig. 3a. The penetration crater depth has been recorded to be 3.6 mm while the simulation yielded a 5.3 mm depth. The recorded spall cone depth is 3.7 mm while the simulation yielded 2.6 mm depth. This leaves a residual thickness of 5.4 mm in the test and 4.8 mm in the simulation of the fused silica pane. HITF13244 performed with a 1.4 mm Al2017-T4 at 9.89 km/s is compared to an Al simulation with a 1.4 mm projectile at 9.89 km/s in Fig 3b. The penetration crater depth has been recorded to be 3.4 mm while the simulation yielded a 4.5 mm depth. The recorded spall cone depth is 1.6 mm while the simulation yielded 1.7 mm depth. This leaves a residual thickness of 7.7 mm in the test and 6.5 mm in the simulation of the fused silica pane. HITF13245 performed with a 1.0 mm SS 440C at 9.56 km/s is compared to a SS simulation with a 1.0 mm projectile at 9.56 km/s in Fig. 3c. The penetration crater depth has been recorded to be 5.0 mm while the simulation yielded a 5.4 mm depth. The recorded spall cone depth is 2.4 mm while the simulation yielded 2.6 mm depth. This leaves a residual thickness of 5.3 mm in the test and 4.7 mm in the simulation of the fused silica pane.

With the favorable comparison between the impact tests and the simulations, a series of simulations have been performed to extend the impact speeds to levels beyond those that have been tested and are summarized in Table 3. The table includes the simulations for nylon, Al and SS from 4 km/s to 30 km/s. The pass is defined in the same manner at the test comparison with simulations carried out to at least 25 μs dependent on no continued evolution of the crater with time; whereas, the fail is progressing through to a hole in the target.

a) b) c)

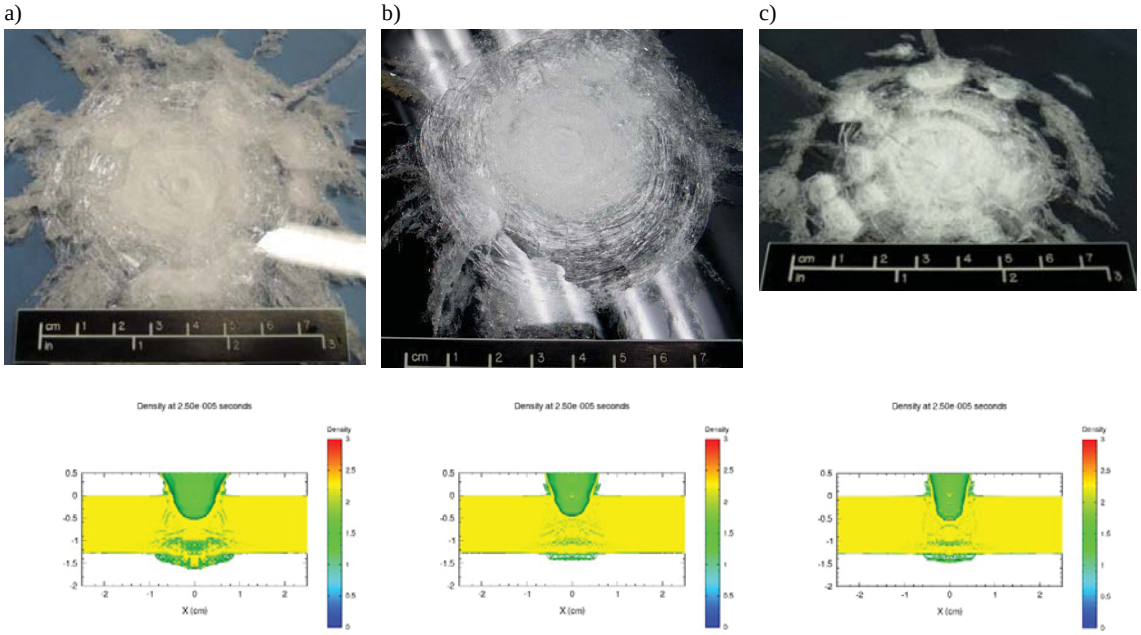


**HITF13243**
2.4 mm Nylon @ 9.23 km/s & 0°

$P_{Sim}$ = 5.3 mm $S_{Sim}$ = 2.6 mm
$P_{Test}$ = 3.6 mm $S_{Test}$ = 3.7 mm

**HITF13244**
1.4 mm Al @ 9.89 km/s & 0°

$P_{Sim}$ = 4.5 mm $S_{Sim}$ = 1.7 mm
$P_{Test}$ = 3.4 mm $S_{Test}$ = 1.6 mm

**HITF13245**
1.0 mm SS @ 9.56 km/s & 0°

$P_{Sim}$ = 5.4 mm $S_{Sim}$ = 2.6 mm
$P_{Test}$ = 5.0 mm $S_{Test}$ = 2.4 mm

Fig. 3 Imagery of the window assembly high velocity tests with simulation comparisons.

Table 3 Fused silica pane impact simulation study to 30 km/s.

| Impact Speed (km/s) | Nylon Pass Diameter (cm) | Nylon Fail Diameter (cm) | Al Pass Diameter (cm) | Al Fail Diameter (cm) | SS Pass Diameter (cm) | SS Fail Diameter (cm) |
|---|---|---|---|---|---|---|
| **4** | 0.42 | 0.5 | 0.26 | 0.3 | 0.18 | 0.2 |
| **7** | 0.32 | 0.36 | 0.18 | 0.22 | 0.13 | 0.15 |
| **10** | 0.27 | 0.31 | 0.18 | 0.22 | | |
| **15** | 0.22 | 0.26 | 0.14 | 0.18 | 0.08 | 0.1 |
| **20** | 0.19 | 0.23 | 0.14 | 0.18 | 0.07 | 0.09 |
| **30** | 0.15 | 0.19 | 0.1 | 0.14 | 0.06 | 0.08 |

## 4. Discussion

The residual depths from Fig. 2 have been fit to the independent impact conditions of target thickness and impactor diameter, density, speed and obliquity to yield a best fit equation for the residual thicknesses, $R$, given by

$$R = 1.93\, t_G - 7.28\, d_i \left(\frac{\rho_i}{\rho_G}\right)^{0.4} \left(\frac{u_i}{c_G}\right)^{0.485} Cos[\theta_i]^{0.05} \quad (1)$$

where $t_G$, $d_i$, $\rho_i$, $\rho_G$, $c_G$, $u_i$ and $\theta_i$ are the thickness of the glass, the diameter and density of the impactor, density (2.2 g/cm$^3$) and sound speed (4.54 km/s) of the glass, the impact speed and obliquity, respectively. These calculated residuals from the fitted equation are tabulated and compared to the measured values in Table 4 for each of the thirteen shots. As the desired condition is perforation, the residual thickness can be set to zero and solved for the projectile diameter that achieves perforation yielding the ballistic limit equation

$$d_c = 0.265\, t_G \left(\frac{\rho_i}{\rho_G}\right)^{-0.4} \left(\frac{u_i}{c_G}\right)^{-0.485} Cos[\theta_i]^{-0.05}. \quad (2)$$

This equation is shown as a solid line relative to the data collected in Fig. 4 with test data drawn as diamonds and simulation data drawn as disks. When the simulation or test indicated an intact shield (pass), the disk or diamond is shown as open; a simulation or a test that yields a perforated fused silica pane is shown filled. In the figure, blue is Al2017-T4, red is nylon and green is SS440C. The dashed lines show the heritage ballistic limit equation [4-5] given by

$$d_c = \left(1.019\, t_G\, \rho_i^{-1/2}\, (u_i\, Cos[\theta_i])^{-2/3}\right)^{1/1.06}. \quad (3)$$

Fig. 4a shows normal impacts into the glass target, and Fig. 4b shows 45° to normal impacts into the glass target. As can be seen all of the tests are accurately determined using this ballistic limit equation including the degree to which the test condition passed. It can also be seen that the simulated points above the testable regime also trend with this ballistic equation, although, absolute values of the curve for the different materials may be slightly different. It is noted that the impact obliquity dependence is very weak for the residual thickness, but this is based off of limited test conditions leaving room for future consideration. The dependence on the projectile density is a somewhat common observation of materials; however, with additional data it is likely that a more involved material description is necessary to account for all materials accurately.

Table 4 Summary of projectile impact conditions and resultant target residual thicknesses.

| **HITF Number** | **Projectile Diameter (cm)** | **Projectile Density (g/cm$^3$)** | **Impact Speed (km/s)** | **Impact Angle (°)** | **Residual Thickness (mm)** | **Calculated Thickness (mm)** |
|---|---|---|---|---|---|---|
| **HITF13243** | 0.238 | 1.146 | 9.23 | 0° | 5.4 | 5.5 |
| **HITF13244** | 0.14 | 2.796 | 9.89 | 0° | 7.7 | 7.9 |
| **HITF13245** | 0.1 | 7.8 | 9.56 | 0° | 5.3 | 7.0 |
| **HITF14075** | 0.318 | 1.146 | 7.15 | 0° | 4.7 | 2.2 |
| **HITF14076** | 0.28 | 2.796 | 3.97 | 0° | 2.8 | 3.4 |
| **HITF14077** | 0.2 | 2.796 | 7.00 | 0° | 5.4 | 4.6 |
| **HITF14078** | 0.25 | 2.796 | 7.04 | 45° | 0.2 | 0.1 |
| **HITF14079** | 0.358 | 1.146 | 7.16 | 0° | Perforation | -0.6 |
| **HITF14080** | 0.358 | 1.146 | 7.14 | 45° | Perforation | -0.1 |
| **HITF14081** | 0.14 | 7.8 | 4.11 | 0° | 8.4 | 7.4 |
| **HITF14082** | 0.25 | 2.796 | 7.23 | 0° | Perforation | -0.6 |
| **HITF14083** | 0.28 | 2.796 | 7.10 | 45° | Perforation | -0.3 |
| **HITF14084** | 0.22 | 2.796 | 7.23 | 0° | 2.7 | 2.3 |

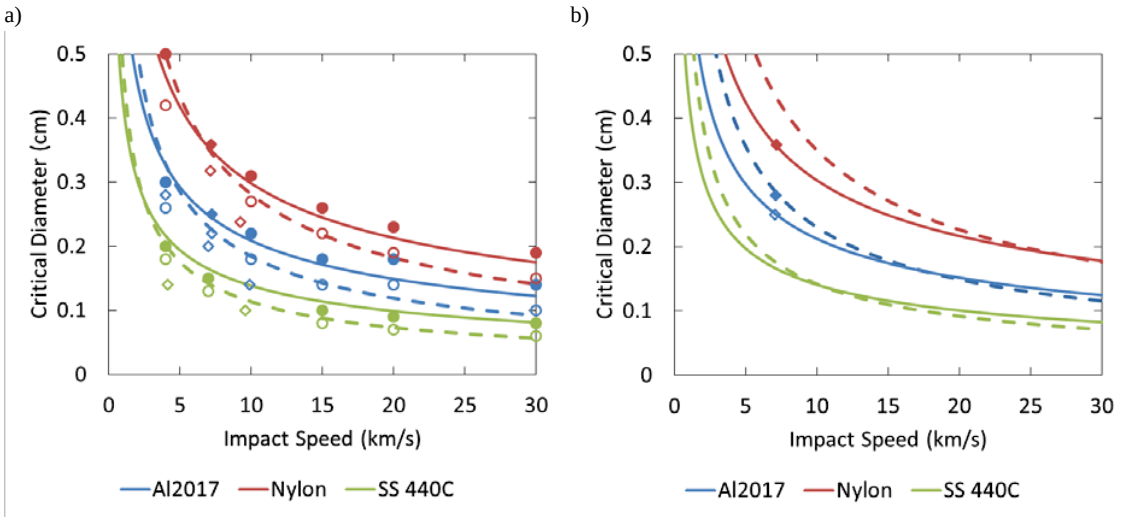


Fig. 4 Accumulated impact test (diamond) and simulation (disk) data with perforated glass shaded and intact glass open along with the revised ballistic model (dashed line) and heritage ballistic model (solid line) for a) normal impacts and b) 45° to normal impacts.

## 5. Conclusion

Through this effort a significant amount of hypervelocity impact data has been developed and synthesized for the MPCV window assembly to the level of perforation. A total of thirteen impact tests have been performed with rapid convergence on the perforation threshold of the fused silica window pane under the impact conditions considered. In addition to the tests performed, a fused silica window pane CTH simulation model has been developed, tested against impact data, and exercised in ballistic data extension. All of the collected test and simulation data have been synthesized using an approach of diminishing residual thickness to produce a ballistic limit equation for use in risk assessments of the Orion spacecraft.

Despite the success of this campaign, continued refinement remains to be performed including the further study on the conclusions of obliquity angle dependence. In addition, more consideration of the effects of the various densities is also needed, and it is especially needed with respect to the higher density parts of the environment like the steel examined here. Further test and simulation work could also be performed to understand the failure threshold to spallation or perforation of the acrylic pane if failure expectations are relaxed.

## References

[1] Christiansen, E. L. Meteoroid/Debris shielding. NASA/TP-2003-210788, National Technical Information Service, Springfield, VA, 2005.
[2] Piekutowski, A. J. and Poormon, K. L. Development of a three-stage, light-gas gun at the University of Dayton Research Institute. Prepared for the 2005 Hypervelocity Impact Symposium, 10-14 October 2005, Lake Tahoe, CA, published in the International Journal of Impact Engineering, 33, 615-624, 2006.
[3] Taylor, E. A., Tsemblis, K., Hayhurst, C. J., Kay, L. and Burchell, M. J. Hydrocode modelling of hypervelocity impact on brittle materials: depth of penetration and conchodial diameter. International Journal of Impact Engineering, 23, 895-904, 1999.
[4] Flaherty, R. E. Impact characteristics in fused silica for various projectile velocities. J. Spacecraft Rockets, 7, 3, 319-324, 1970.
[5] Christiansen, E. L. Handbook for designing MMOD protection. NASA/TP-2009-214785, National Technical Information Service, Springfield, VA, 2009.